Appl. Phys. A (2014) 117:1367–1374
DOI 10.1007/s00339-014-8557-2

Applied Physics A
Materials Science & Processing

Simulation of thermionic emission optimization in femtosecond laser irradiation metal film by two-layer structure

Jin Guo · Tingfeng Wang · Dinan Wang · Junfeng Shao · Anmin Chen · Mingxing Jin

Received: 27 December 2013 / Accepted: 11 June 2014 / Published online: 22 June 2014

Abstract The thermionic emission of the single-layer gold thin film and the two-layer film was assembled by gold padded with other metals (Ag, Cu, and Ni) and irradiated by the femtosecond laser pulse. Additionally, the emission was simulated by a two-temperature model combined with the Richardson–Dushman equation. It was found that the two-layer metal structure can change the electron temperature of the gold surface and control the thermionic emission compared with the single-layer gold film. With the same laser fluence, the two-layer film structure may shorten the duration of thermionic emission, and the duration of the thermionic emission can be further optimized by changing the proportion of thin film thickness with gold layer in the two-layer structure. The result can be especially beneficial in the context of ultrafast electron emission induced by femtosecond laser.

J. Guo · T. Wang · D. Wang · J. Shao
State Key Laboratory of Laser Interaction with Matter, Changchun Institute of Optics, Fine Mechanics and Physics, Chinese Academy of Sciences, Changchun 130033, China

A. Chen (✉) · M. Jin (✉)
Institute of Atomic and Molecular Physics, Jilin University, Changchun 130012, China
e-mail: comeongoon@sohu.com

M. Jin
e-mail: mxjin@jlu.edu.cn

A. Chen
State Key Laboratory of Theoretical and Computational Chemistry, Institute of Theoretical Chemistry, Jilin University, Changchun 130012, China

1 Introduction

The interaction of femtosecond laser pulses with metals has become the topic of most concerns thanks to its increasing significance and contribution in many applications [1–4]. Femtosecond laser irradiation metal is a complex process [5]. When the metal surface is irradiated by a femtosecond laser pulse, the electron temperature tends to increase rapidly in an extremely short period of time since specific heat capacity of the electron is very low. Consequently, the great temperature difference between electron and lattice is generated. The nonequilibrium energy transport of electron and lattice will take place on account of the electron–lattice coupling mechanism [6]. Based on the nonequilibrium electron heating process, laser-induced electron emission tends to give rise to several applications, such as laser driven electron sources [7, 8] and ultrashort x-ray pulses [9, 10]. Additionally, the produced electron emission has also been widely used for plasma diagnostics [11, 12], excited electron lifetimes [13], ultrafast electron dynamics in metallic surfaces [14, 15], surface states [16, 17], and so forth.

The femtosecond laser-induced ultrafast electron pulse can be generated by the optical field emission [18, 19] or the photoemission [20, 21]. Both of the processes of produced electron emission will be inevitably attached to the thermionic emission [22] under femtosecond laser pulse irradiation. The mechanism of thermionic emission with femtosecond laser irradiation metal has been studied by many researchers [23, 24]. The tailing phenomenon of the thermionic emission can be observed in the published data [25, 26]. In the applications of ultrafast electron emission, people consider that the duration of electron emission is much shorter. Therefore, the studies on the reduced tailing phenomenon and decreased thermionic

emission duration are of great importance to the applications of the ultrafast electron emission. On the grounds of physical mechanism of thermionic emission [27, 28], the thermionic electron emission comes from the metal surface electrons with the higher temperature, and these electrons can overcome the potential energy barrier. The number of emitted electrons is determined by the electron temperature [29]. By decreasing the electron temperature of metal surface after laser irradiation, the thermal energy of electrons cannot overcome the binding potential, also known as the work function of metal. The tailing phenomenon of thermionic emission, therefore, can be reduced.

Due to the nonequilibrium process of femtosecond laser heating metal, some researchers started to work on the electron dynamics mechanism in two-layer metal films which is irradiated by femtosecond pulsed laser [30–32]. By the two-layer structure, the electron temperature of metal surface can be obviously reduced after femtosecond laser irradiation so that the thermionic emission can be optimized. In this paper, the two-layer structure was introduced into the thermionic emission under femtosecond laser irradiation. In addition, femtosecond laser heating of the single-layer gold or the two-layer gold padded with other metal materials, such as silver, copper, and nickel, was investigated numerically. The predicted results indicated that the additional layer metal can accelerate the decay of surface electron temperature. Furthermore, the thermionic emission of gold surface will be optimized accordingly. The study can be especially advantageous in the context of femtosecond laser-induced ultrafast electron emission.

2 Mathematical model

2.1 Two-temperature model

The period of time for the action that metals are heated with femtosecond laser pulses is significantly much less than electron–lattice relaxation time. Therefore, when calculating the temperature, it is necessary to adopt the two-temperature model (TTM) [33–35] which takes into account the heating of electron subsystem relative to the lattice subsystem. The radiation energy is initially absorbed by free electrons and then transferred to the lattice. The lattice is therefore already heated by the pulse ends. The one-dimension two-temperature equation is given below [36–38]

$$C_{\mathrm{e}}\frac{\partial T_{\mathrm{e}}}{\partial t}=\frac{\partial}{\partial x}\left(k_{\mathrm{e}}\frac{\partial T_{\mathrm{e}}}{\partial x}\right)-G(T_{\mathrm{e}}-T_{\mathrm{l}})+S \tag{1}$$

$$C_{\mathrm{l}}\frac{\partial T_{\mathrm{l}}}{\partial t}=\frac{\partial}{\partial x}\left(k_{\mathrm{l}}\frac{\partial T_{\mathrm{e}}}{\partial x}\right)+G(T_{\mathrm{e}}-T_{\mathrm{l}}) \tag{2}$$

where C stands for the volumetric heat capacity, k is the thermal conductivity, T represents the temperature, G is the electron–lattice coupling constant [39], t is the time, and x is the depth. The subscripts e and l represent the electron and lattice, respectively. The heat source S can be modeled with a Gaussian temporal profile [40]

$$S=\sqrt{\frac{\beta}{\pi}}\frac{(1-R)I}{t_{\mathrm{p}}\alpha}\exp\left[-\frac{x}{\alpha}-\beta\left(\frac{t-2t_{\mathrm{p}}}{t_{\mathrm{p}}}\right)^2\right] \tag{3}$$

where R is the target reflection coefficient, t_{p} is the full width at the half maximum (FWHM) with the linear polarization, α is the penetration depth including the ballistic range, I is the incident energy, and $\beta=4\ln(2)$.

The electron heat capacity is proportional to the electron temperature when the electron temperature is less than the Fermi temperature as $C_{\mathrm{e}}=\gamma T_{\mathrm{e}}$ [41] and $\gamma=\pi^2 n_{\mathrm{e}}k_{\mathrm{B}}/2T_{\mathrm{F}}$. n_{e} is the density of the free electrons, and k_{B} is the Boltzmann's constant. The lattice heat capacity can be set as a constant due to its relatively small variation as the temperature changes. As the temperature changes, the variety of lattice heat capacity is relatively small, which is considered as a constant.

The electron heat conductivity can be expressed as $k_{\mathrm{e}}=k_{\mathrm{e0}}BT_{\mathrm{e}}/(AT_{\mathrm{e}}^2+BT_{\mathrm{l}})$ [42], where k_{e0}, A, and B are material constants. The lattice thermal conductivity is therefore regarded as 1 % of the thermal conductivity of bulk metal since the mechanism of heat conduction in metal mainly depends on electrons [43].

Many of the ultrafast laser heating analyses are carried out with constant electron–lattice coupling factor G. However, due to the significant changes in electron and lattice temperatures induced by high-power laser heating, G should be considered as a temperature dependent ($G=G_0(A(T_{\mathrm{e}}+T_{\mathrm{l}})/B+1)$, where G_0 is the coupling factor at room temperature) [44, 45].

For the two-layer structure, the position of the interface is $x=l$. For the two-layer thin film, the two-temperature equation (Eqs. 1, 2) for studying thermal behavior in the two-layer metal thin film can be expressed as follows: [46]

$$C_{\mathrm{e}}^{I}\frac{\partial T_{\mathrm{e}}^{I}}{\partial t}=\frac{\partial}{\partial x}\left(k_{\mathrm{e}}^{I}\frac{\partial T_{\mathrm{e}}^{I}}{\partial x}\right)-G\left(T_{\mathrm{e}}^{I}-T_{\mathrm{l}}^{I}\right)+S^{I} \tag{4}$$

$$C_{\mathrm{l}}^{I}\frac{\partial T_{\mathrm{l}}^{I}}{\partial t}=\frac{\partial}{\partial x}\left(k_{\mathrm{l}}^{I}\frac{\partial T_{\mathrm{l}}^{I}}{\partial x}\right)+G\left(T_{\mathrm{e}}^{I}-T_{\mathrm{l}}^{I}\right) \tag{5}$$

$$C_{\mathrm{e}}^{II}\frac{\partial T_{\mathrm{e}}^{II}}{\partial t}=\frac{\partial}{\partial x}\left(k_{\mathrm{e}}^{II}\frac{\partial T_{\mathrm{e}}^{II}}{\partial x}\right)-G\left(T_{\mathrm{e}}^{II}-T_{\mathrm{l}}^{II}\right) \tag{6}$$

$$C_{\mathrm{l}}^{II}\frac{\partial T_{\mathrm{l}}^{II}}{\partial t}=\frac{\partial}{\partial x}\left(k_{\mathrm{l}}^{II}\frac{\partial T_{\mathrm{l}}^{II}}{\partial x}\right)+G\left(T_{\mathrm{e}}^{II}-T_{\mathrm{l}}^{II}\right) \tag{7}$$

2.2 Thermionic emission

If the temperature of conduction electrons in metal is high enough, the tail part of the Fermi–Dirac distribution leaks into the vacuum level, resulting in thermionic electron emission. The rate of thermionic emission from metal is represented by the Richardson–Dushman equation [47–49].

$$J = \left(\frac{4\pi m}{h^3}\right)(k_B T_e)^2 \exp\left[-\frac{e\varphi}{k_B T_e}\right] \tag{8}$$

where k_B is the Boltzmann constant, φ is the work function of the metal [50], m is the mass of the electron, and h is the Planck constant. In the equation, the photoemission is ignored. According to the physical mechanism of the photoemission, the photoemission will not generate the tailing phenomenon after femtosecond laser irradiation.

2.3 Initial and boundary conditions

In order to solve Eqs. (4, 5, 6, 7), the electron and lattice subsystems are considered to be at the same initial temperature ($T_0 = 300$ K). The initial conditions are as follows:

$$T_e^I(x,0) = T_l^I(x,0) = T_0 \tag{9}$$

$$T_e^{II}(x,0) = T_l^{II}(x,0) = T_0 \tag{10}$$

The boundary conditions are as follows:

$$\left.\frac{\partial T_e^I}{\partial x}\right|_{x=0} = -J(e\phi) \tag{11}$$

$$\left.\frac{\partial T_e^{II}}{\partial x}\right|_{x=L} = 0 \tag{12}$$

$$\left.\frac{\partial T_l^I}{\partial x}\right|_{x=0} = \left.\frac{\partial T_l^{II}}{\partial x}\right|_{x=L} = 0 \tag{13}$$

At the interface of the film ($x = l$), the two-layer thin film is in perfect thermal contact. Therefore, we set the boundary conditions of the interface as follows:

$$T_e^I|_{x=l} = T_e^{II}|_{x=l} \tag{14}$$

$$T_l^I|_{x=l} = T_l^{II}|_{x=l} \tag{15}$$

$$k_e^I \left.\frac{\partial T_e^I}{\partial x}\right|_{x=l} = k_e^{II} \left.\frac{\partial T_e^{II}}{\partial x}\right|_{x=l} \tag{16}$$

$$k_l^I \left.\frac{\partial T_l^I}{\partial x}\right|_{x=l} = k_l^{II} \left.\frac{\partial T_l^{II}}{\partial x}\right|_{x=l} \tag{17}$$

3 Result and discussion

The laser light source employed in the simulation process was a 100-fs laser with the wavelength of 800 nm. The surface reflectivity of gold was $R = 0.974$. The values of the thermal physical parameters adopted in these calculations are listed in Table 1 [51–55]. Figure 1 shows the comparison of normalized calculated electron temperature and normalized experimental transient reflectivity [56] under femtosecond pulse laser irradiation. The laser fluence was 6 mJ cm^{-2}. The change in electron temperature (ΔT_e) directly was related to the change in the reflectivity ($\Delta R/R$). The expression was $\Delta R/R = a\Delta T_e$ [56–58], and the coefficient a was a constant. Figure 1 presents a reasonable agreement between the numerical result and the experiment result. Therefore, it was convinced that the numerical simulation method is credible.

Table 1 Physical parameters for the four metals

	Au	Ag	Cu	Ni
G_0 (10^{17} Jm^{-3} s^{-1} K^{-1})	0.21	0.31	1.0	3.6
γ (Jm^{-3} K^{-2})	68	63	97	1,065
k_{e0} (Jm^{-1} s^{-1} K^{-1})	318	428	401	90
C_l (10^6 Jm^{-3} K^{-1})	2.5	2.5	3.5	4.1
α (10^{-9} m)	13.7	12.9	12.2	13.5
A (10^7 s^{-1} K^{-2})	1.18	0.932	1.28	0.59
B (10^{11} s^{-1} K^{-1})	1.25	1.02	1.23	1.4

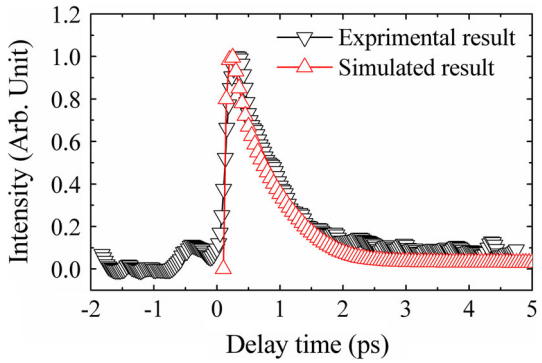

Fig. 1 The comparison of simulated and experimental results

The time dependence of calculated electron temperature on the surface of single-layer gold is demonstrated in Fig. 2a. The thickness of single-layer gold film was 200 nm. The laser fluence was 50, 100, 500, and 1,000 mJ cm^{-2}, respectively. We can see from this plot that electron temperature rose rapidly at the surface region, with that attained the maximum of surface electron temperature. After femtosecond laser irradiation, the surface electron temperature decreased with the delay time due to the effect of heat diffusion in the free electron gas [38, 42]. The decay time of electron temperature increased along with the increase of femtosecond laser fluence. Figure 2b shows the temporal evolution of thermionic emission calculated from Fig. 2a and Eq. (8). It indicated that the peak intensity of the thermionic emission was significantly

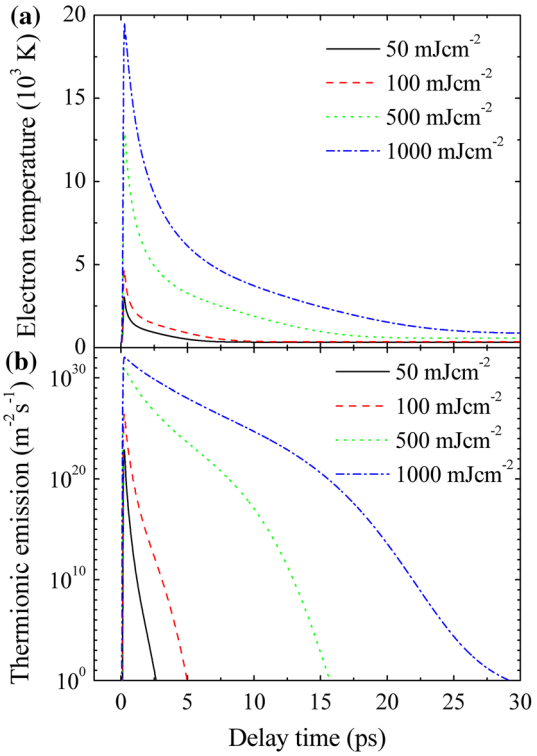

Fig. 2 The evolution of electron temperature (**a**) and thermionic emission (**b**) with the delay time at the different laser fluence. The thickness of single-layer gold is 200 nm. The laser fluence is 50, 100, 500, and 1,000 mJ cm^{-2}, respectively

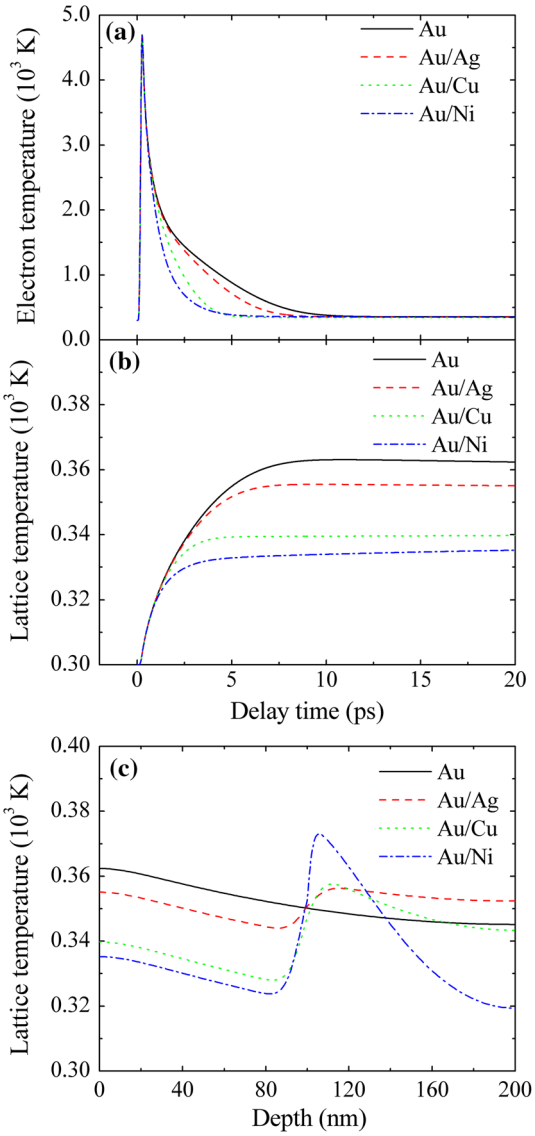

Fig. 3 The evolution of electron temperature (**a**) and lattice temperature (**b**) with the delay time at the surface, the distribution of lattice temperature (**c**) with the depth at the delay time of 20 ps for single-layer Au film (200 nm), Au/Ag two-layer film (100 nm Au and 100 nm Ag), Au/Cu two-layer film (100 nm Au and 100 nm Cu), and Au/Ni two-layer film (100 nm Au and 100 nm Ni). The laser fluence is 100 mJcm^{-2}

increased by increasing the laser fluence. The tailing of thermionic emission was obviously prolonged with the increase of laser fluence [25, 48, 59].

In general, the thermal parameters for metals are physically originated from free electron thermal movement and coupling of electron–lattice in the metal [35, 36]. For two-layer metal film, the thermal parameters, such as the electron–lattice coupling strength, can vary significantly with different layers of the assembly [30, 31]. The two-layer metal film under femtosecond pulse laser irradiation would take on the different thermal behavior of the electron and lattice for the different substrate metal [46]. Therefore, the variation of electron temperature will be affected accordingly. The electrons with higher temperature lead to thermionic emission. And the corresponding thermionic emission of the two-layer metal film will be largely affected by changing the substrate metal.

Figure 3a, b shows the variation of electron temperature and lattice temperature at the surface with the delay time for the single-layer gold film and the gold-coated two-layer metal films irradiated by femtosecond pulse laser. The laser fluence was 100 mJ cm^{-2}. The thickness of the single-layer gold film was 200 nm. The two-layer metal film was a 100-nm-thick gold layer padding on a 100-nm-thick silver layer, a 100-nm-thick copper layer, and a 100-nm-thick nickel layer, respectively. In Fig. 3a, the electron temperature rose rapidly at the metal film surface, attaining all surface electron temperature maximum with 4,696 K for Au, Au/Ag, Au/Cu, and Au/Ni. The surface electron temperature decreased along with the time due to the heat diffusion effect of free electron gas in a very short delay time (about 1 ps). With the increase of the delay time, the distributions of the surface electron temperature for four different metal film assemblies were already noticeably different. The decay rate of electron temperature of single-

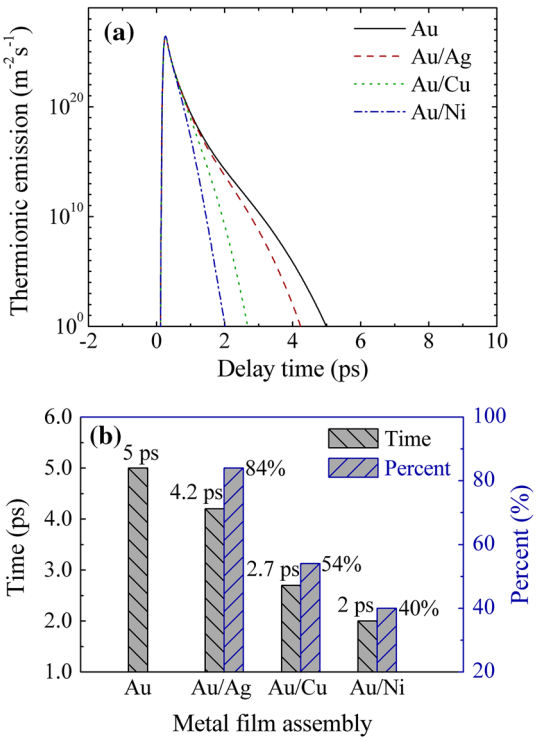

Fig. 4 **a** The evolution of thermionic emission with the delay time for single-layer Au film (200 nm), Au/Ag two-layer film (100 nm Au and 100 nm Ag), Au/Cu two-layer film (100 nm Au and 100 nm Cu), and Au/Ni two-layer film (100 nm Au and 100 nm Ni). The laser fluence is 100 mJ cm^{-2}. **b** comparison of electron emission duration (*left axes*) and percentage (*right axes*)

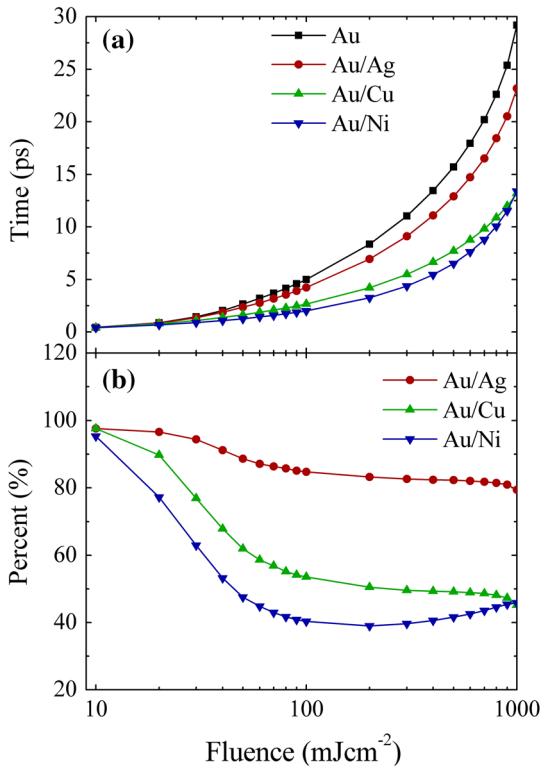

Fig. 5 The evolution of the thermionic emission (**a**) and the changed ratio (**b**) with the laser fluence for single-layer Au film (200 nm), Au/Ag two-layer film (100 nm Au and 100 nm Ag), Au/Cu two-layer film (100 nm Au and 100 nm Cu), and Au/Ni two-layer film (100 nm Au and 100 nm Ni). The laser fluence is 50, 100, 500, and 1,000 mJ cm^{-2}, respectively

layer gold film was less than that of the two-layer metal film. And, the two-layer structure also reduced the gold surface lattice temperature, as shown in Fig. 3b. Figure 3c shows the distribution of lattice temperature with the depth at the delay time of 20 ps. It was noticed that the distribution of lattice temperature had big ups and downs in the interface region of the two-layer films. At the range from 0 to 100 nm, the lattice temperature of single-layer gold film was higher than that of two-layer films. In the case of the two-layer assemblies, at first, electrons established an extended energy deposition depth in the gold layer [39, 40]. Then, these electrons penetrated into the padding layer and started to couple their energy to the lattice. The coupling efficiency of the padding layer was much faster than the counterparts in the top gold layer due to large electron–lattice coupling coefficient (shown in Table 1). The effect resulted in reducing electron temperature of gold surface. The rapid decay rate of the electron temperature would reduce the duration of the thermionic emission tailing.

The thermionic emission of gold-coated two-layer metal film surface calculated from Fig. 3a and Eq. (8) is clearly presented in Fig. 4a. As can be seen from this figure, the tailing phenomenon of thermionic electron emission irradiated under femtosecond laser pulse was obviously reduced by the two-layer structure. The duration of electron emission of four metal films (including Au, Au/Ag, Au/Cu, and Au/Ni) was 5, 4.2, 2.7, and 2 ps, respectively. As shown in Fig. 4b, among three gold-coated two-layer metal films, Au/Ni was the most effective assembly (the electron–lattice coupling coefficient is largest). The duration of the thermionic emission tailing was reduced to 40 % compared with the single-layer gold. In the process of femtosecond laser heating metal film, electron temperature became very high at the surface by absorbing laser energy, resulting in large electron thermal conductivity [34, 42]. Therefore, electrons could quickly transfer energy to the internal electrons of second-layer metal. The reason for that was the second-layer metal had larger electron–lattice coupling coefficient (G), and the energy was then rapidly transferred to the lattice of the second-layer metal. An increase of electron temperature gradient was present [60, 61], resulting in faster electron energy transfer. The surface electron temperature of gold layer would therefore be reduced. The second-layer tended to serve as an energy sink absorbing the thermal energy of the first-layer

electrons. It may accelerate the decay of surface electron temperature, and the duration of the thermionic emission tailing was reduced.

With that, we calculated the duration of the thermionic electron emission with the laser fluence. Figure 5a shows that the duration of the thermionic emission of gold for single-layer and two-layer films increased monotonically with the laser fluence. In comparison with the single-layer metal film, the increase of the duration was much slower for the two-layer metal films. Meanwhile, the duration of single-layer gold was longer than the duration of the gold-coated two-layer film. The ratio of thermionic emission duration of the gold-coated two-layer film to the single-layer gold was calculated through the duration of two-layer film divided by the duration of single-layer gold, as shown in Fig. 5b. The ratio decreased with the laser fluence in the range from 10 to 100 mJ cm^{-2}. Continue to increase the laser fluence, the ratio was almost constant. For Au/Ag two-layer film, the thermal parameters (Table 1) between Au and Ag were very close to each other so that the ratio of Au/Ag two-layer film was above 80 %. However, the ratio of Au/Cu and Au/Ni may even reach around 50 % for the higher laser fluence.

Above the section, we mainly discussed the effect of the laser fluence for the duration of the thermionic emission at the fixed proportion of thin film thickness of gold layer (100 nm) and substrate layer metals (100 nm). Next, the evolution of gold-coated two-layer metal thermionic emission with the thickness of the gold layer thin film was investigated. The thickness of the gold layer was l, changing between 50 nm and 150 nm. The interval was 10 nm. The thickness of the substrate layer was $L - l$ ($L = 200$ nm). Figure 6 shows the duration of the thermionic emission as a function of the thickness of the gold layer for four laser fluence (including 50, 100, 500, and 1,000 mJ cm^{-2}). It is clearly suggested that the increase of laser fluence could wholly lead to the significant increase of the duration of the thermionic emission for the three different two-layer metal film assemblies. At higher laser fluence, the duration of electron emission was reduced obviously by decreasing the thickness of the gold layer for two-layer metal films of Au/Ag and Au/Cu. However, for the high laser fluence (1,000 mJ cm^{-2}), compared with Au/Ag and Au/Cu, the abnormal change on the Au/Ni could be observed. In the thermal physical parameters of Ni (Table 1), the electron heat conductivity was low compared with the other metals (Au, Ag, and Cu). When the laser fluence was higher, the energy of the laser heating electron could not be transferred quickly [1, 44]. So that electron of gold surface electron was at a higher temperature in a relatively long time [38]. Therefore, it can be concluded that we should not only choose the metals with the large electron–lattice coupling coefficient as the second-layer of two-layer metal film, but also choose the metals with large electron heat conductivity.

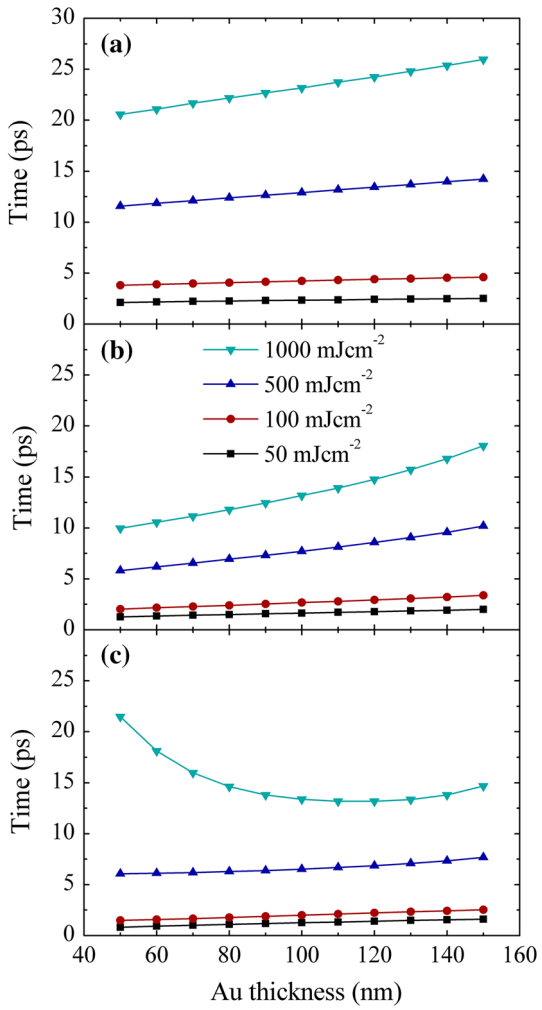

Fig. 6 The evolution of electron emission duration with the thickness of gold layer for the different laser fluence: **a** Au/Ag two-layer film, **b** Au/Cu two-layer film, and **c** Au/Ni two-layer film. The laser fluence is 50, 100, 500, and 1,000 mJ cm^{-2}, respectively

4 Conclusion

In conclusion, a numerical solution of the two-temperature model combined with the Richardson–Dushman equation had been performed up to the thermionic emission of femtosecond laser-heated single-layer gold film and the gold-coated two-layer metal films. For the same laser fluence, the single-layer gold film and the two-layer metal films (including Au/Ag, Au/Cu, and Au/Ni) would lead to the different evolution of gold surface electron temperature and the corresponding duration of thermionic electron emission. The gold-coated two-layer metal films could shorten the duration of electron emission compared with the single-layer gold film. At the higher laser fluence, the

duration of the thermionic emission tailing was reduced to around 50 % by the two-layer structure. Additionally, the duration of thermionic emission could be further optimized by changing the proportion of thin film thickness of gold layer in the two-layer structure. Besides, as choosing the second-layer metal, not only the metals with large electron–lattice coupling coefficient as the second-layer of two-layer metal film should be chosen, but also the metals with large electron heat conductivity. This result could optimize the thermionic electron emission in the applications of ultrafast electron beam source generated by femtosecond laser irradiation metal.

Acknowledgments This project was supported by the Fundamental Research Funds for the Central Universities, the China Postdoctoral Science Foundation (Grant no. 2014M551169), the National Basic Research Program of China (973 Program, Grant No. 2013CB922200), and the National Natural Science Foundation of China (Grant Nos. 10974069 and 11034003).

References

1. A.V. Lugovskoy, I. Bray, Phys. Rev. B **65**, 3279 (1999)
2. C. Kealhofer, S.M. Foreman, S. Gerlich, M.A. Kasevich, Phys. Rev. B **86**, 035405 (2012)
3. Z.Y. Chen, J.F. Li, Y. Yu, J.X. Wang, X.Y. Li, Q.X. Peng, W.J. Zhu, Phys. Plasmas **19**, 113116 (2012)
4. L.M. Chen, J. Zhang, Q.L. Dong, H. Teng, T.J. Liang, L.Z. Zhao, Z.Y. Wei, Phys. Plasmas **8**, 2925 (2001)
5. B. Rethfeld, K. Sokolowski-Tinten, D. von der Linde, S.I. Anisimov, Appl. Phys. Mater. Sci. Process. **79**, 767 (2004)
6. B.H. Christensen, K. Vestentoft, P. Balling, Appl. Surf. Sci. **253**, 6347 (2007)
7. V. Ayvazyan, N. Baboi, I. Bohnet, R. Brinkmann, M. Castellano, P. Castro, L. Catani, S. Choroba, A. Cianchi, M. Dohlus, H.T. Edwards, B. Faatz, A.A. Fateev, J. Feldhaus, K. Flottmann, A. Gamp, T. Garvey, H. Genz, C. Gerth, V. Gretchko, B. Grigoryan, U. Hahn, C. Hessler, K. Honkavaara, M. Huning, R. Ischebeck, M. Jablonka, T. Kamps, M. Korfer, M. Krassilnikov, J. Krzywinski, M. Liepe, A. Liero, T. Limberg, H. Loos, M. Luong, C. Magne, J. Menzel, P. Michelato, M. Minty, U.C. Muller, D. Nolle, A. Novokhatski, C. Pagani, F. Peters, J. Pfluger, P. Piot, L. Plucinski, K. Rehlich, I. Reyzl, A. Richter, J. Rossbach, E.L. Saldin, W. Sandner, H. Schlarb, G. Schmidt, P. Schmuser, J.R. Schneider, E.A. Schneidmiller, H.J. Schreiber, S. Schreiber, D. Sertore, S. Setzer, S. Simrock, R. Sobierajski, B. Sonntag, B. Steeg, F. Stephan, K.P. Sytchev, K. Tiedtke, M. Tonutti, R. Treusch, D. Trines, D. Turke, V. Verzilov, R. Wanzenberg, T. Weiland, H. Weise, M. Wendt, I. Will, S. Wolff, K. Wittenburg, M.V. Yurkov, K. Zapfe, Phys. Rev. Lett. **88**, 104802 (2002)
8. X.J. Wang, D. Xiang, T.K. Kim, H. Ihee, J. Korean Phys. Soc. **48**, 390 (2006)
9. Z.S. Tao, H. Zhang, P.M. Duxbury, M. Berz, C.Y. Ruan, J. Appl. Phys. **111**, 044316 (2012)
10. J.F. Seely, C.I. Szabo, P. Audebert, E. Brambrink, E. Tabakhoff, L.T. Hudson, Phys. Plasmas **17**, 023102 (2010)
11. P.F. Zhu, Z.C. Zhang, L. Chen, J. Zheng, R.Z. Li, W.M. Wang, J.J. Li, X. Wang, J.M. Cao, D. Qian, Z.M. Sheng, J. Zhang, Appl. Phys. Lett. **97**, 211501 (2010)
12. J.J. Li, X. Wang, Z.Y. Chen, R. Clinite, S.S. Mao, P.F. Zhu, Z.M. Sheng, J. Zhang, J.M. Cao, J. Appl. Phys. **107**, 083305 (2010)
13. V.P. Zhukov, O. Andreyev, D. Hoffmann, M. Bauer, M. Aeschlimann, E.V. Chulkov, P.M. Echenique, Phys. Rev. B **70**, 233106 (2004)
14. P. Hommelhoff, Y. Sortais, A. Aghajani-Talesh, M.A. Kasevich, Phys. Rev. Lett. **96**, 077401 (2006)
15. J. Chen, W.K. Chen, J. Tang, P.M. Rentzepis, Proc. Natl. Acad. Sci. U.S.A. **108**, 18887 (2011)
16. H. Ueba, B. Gumhalter, Prog. Surf. Sci. **82**, 193 (2007)
17. R.D. Muino, D. Sanchez-Portal, V.M. Silkin, E.V. Chulkov, P.M. Echenique, Proc. Natl. Acad. Sci. U.S.A. **108**, 971 (2011)
18. R. Bormann, M. Gulde, A. Weismann, S.V. Yalunin, C. Ropers, Phys. Rev. Lett. **105**, 147601 (2010)
19. H. Yanagisawa, C. Hafner, P. Dona, M. Klockner, D. Leuenberger, T. Greber, J. Osterwalder, M. Hengsberger, Phys. Rev. B **81**, 115429 (2010)
20. J. Faure, J. Mauchain, E. Papalazarou, W. Yan, J. Pinon, M. Marsi, L. Perfetti, Rev. Sci. Instrum. **83**, 043109 (2012)
21. H. Petek, S. Ogawa, Prog. Surf. Sci. **56**, 239 (1997)
22. J.W. Schwede, T. Sarmiento, V.K. Narasimhan, S.J. Rosenthal, D.C. Riley, F. Schmitt, I. Bargatin, K. Sahasrabuddhe, R.T. Howe, J.S. Harris, N.A. Melosh, Z.X. Shen, Nat. Commun. **4**, 1576 (2013)
23. X.Y. Wang, D.M. Riffe, Y.S. Lee, M.C. Downer, Phys. Rev. B **50**, 8016 (1994)
24. D.M. Riffe, X.Y. Wang, M.C. Downer, D.L. Fisher, K. Tajima, J.L. Erskine, J. Opt. Soc. Am. B: Opt. Phys. **10**, 1424 (1993)
25. T. Balasubramni, S.H. Kim, S.H. Jeong, Appl. Surf. Sci. **255**, 9601 (2009)
26. G.Q. Du, Q. Yang, F. Chen, J.H. Si, X. Hou, Appl. Surf. Sci. **257**, 9177 (2011)
27. E.B. Yakovlev, O.N. Sergaeva, V.V. Svirina, J. Opt. Technol. **78**, 487 (2011)
28. S.G. Bezhanov, A.P. Kanavin, S.A. Uryupin, Quantum Electron. **42**, 447 (2012)
29. E.L. Murphy, R.H. Good, Phys. Rev. **102**, 1464 (1956)
30. W.M.G. Ibrahim, H.E. Elsayed-Ali, C.E. Bonner, M. Shinn, Int. J. Heat Mass Transf. **47**, 2261 (2004)
31. A.M. Chen, L.Z. Sui, Y. Shi, Y.F. Jiang, D.P. Yang, H. Liu, M.X. Jin, D.J. Ding, Thin Solid Films **529**, 209 (2013)
32. A.M. Chen, Y.F. Jiang, L.Z. Sui, H. Liu, M.X. Jin, D.J. Ding, J. Opt. **13**, 055503 (2011)
33. S.I. Anisimov, B.L. Kapeliovich, T.L. Perelman, Sov. J. Exp. Theoret. Phys. **39**, 375 (1974)
34. S.Y. Wang, Y. Ren, C.W. Cheng, J.K. Chen, D.Y. Tzou, Appl. Surf. Sci. **265**, 302 (2013)
35. Y. Gan, J.K. Chen, Opt. Lett. **37**, 2691 (2012)
36. Y. Gan, J.K. Chen, Appl. Phys. Lett. **94**, 201116 (2009)
37. P.B. Corkum, F. Brunel, N.K. Sherman, T. Srinivasan-Rao, Phys. Rev. Lett. **61**, 2886 (1988)
38. J.K. Chen, J.E. Beraun, J. Opt. Pure Appl. Opt. **5**, 168 (2003)
39. P.B. Allen, Phys. Rev. Lett. **59**, 1460 (1987)
40. A.A. Unal, A. Stalmashonak, G. Seifert, H. Graener, Phys. Rev. B **79**, 115411 (2009)
41. J. Kim, S. Na, Opt. Laser Technol. **39**, 1443 (2007)
42. Y. Yamashita, T. Yokomine, S. Ebara, A. Shimizu, Fusion Eng. Des. **81**, 1695 (2006)
43. Y.W. Zhang, J.K. Chen, J. Appl. Phys. **104**, 054910 (2008)
44. P.E. Hopkins, P.M. Norris, Appl. Surf. Sci. **253**, 6289 (2007)
45. J. Huang, Y.W. Zhang, J.K. Chen, Appl. Phys. Mater. Sci. Process. **95**, 643 (2009)
46. A.M. Chen, H.F. Xu, Y.F. Jiang, L.Z. Sui, D.J. Ding, H. Liu, M.X. Jin, Appl. Surf. Sci. **257**, 1678 (2010)
47. S.S. Mao, X. Mao, R. Greif, R.E. Russo, Appl. Phys. Lett. **73**, 1331 (1998)
48. G.Q. Du, Q. Yang, F. Chen, X.W. Meng, H. Bian, J.H. Si, X. Hou, Appl. Phys. Mater. Sci. Process. **112**, 479 (2013)

49. J. Guo, T.F. Wang, J.F. Shao, T. Sun, R. Wang, A.M. Chen, Z. Hu, M.X. Jin, D.J. Ding, Opt. Commun. **285**, 1895 (2012)
50. W.M.H. Sachtler, G.J.H. Dorgelo, A.A. Holscher, Surf. Sci. **5**, 221 (1966)
51. S. Amoruso, R. Bruzzese, X. Wang, N.N. Nedialkov, P.A. Atanasov, J. Phys. D Appl. Phys. **40**, 331 (2007)
52. D.R. Lide, *CRC handbook of chemistry and physics*, 84th edn. (CRC Press, Boca Raton, 2003)
53. B.S. Yilbas, Numer. Heat Transf. Part Appl. **52**, 565 (2007)
54. J.J. Yang, W.W. Liu, X.N. Zhu, Chin. Phys. **16**, 2003 (2007)
55. J.A. Sanchez, M.P. Menguc, J. Appl. Phys. **103**, 054316 (2008)
56. A. Chen, L. Sui, Y. Shi, Y. Jiang, D. Yang, H. Liu, M. Jin, D. Ding, Thin Solid Films **529**, 209 (2013)
57. P.E. Hopkins, J.L. Kassebaum, P.M. Norris, J. Appl. Phys. **105**, 023710 (2009)
58. S. Brorson, A. Kazeroonian, J. Moodera, D. Face, T. Cheng, E. Ippen, M. Dresselhaus, G. Dresselhaus, Phys. Rev. Lett. **64**, 2172 (1990)
59. T. Balasubramani, S.H. Jeong, J. Phys.: Conf. Ser. **59**, 595 (2007)
60. T.Q. Qiu, C.L. Tien, Int. J. Heat Mass Transf. **37**, 2789 (1994)
61. A. Karakas, M. Tunc, U. Camdali, Heat Mass Transf. **46**, 1287 (2010)